

# Spectral Edge Dynamics of Training Trajectories: Signal–Noise Geometry Across Scales

Yongzhong Xu\*

## Abstract

Despite hundreds of millions of parameters, transformer training trajectories evolve within only a few coherent directions. We introduce *Spectral Edge Dynamics* (SED) to measure this structure: rolling-window SVD of parameter updates reveals a sharp boundary—the *spectral edge*—between coherent optimization directions and stochastic noise, identified by the maximum consecutive singular value ratio  $\sigma_k/\sigma_{k+1}$ . Across a 51M-parameter TinyStories model (4 seeds) and GPT-2 124M under a distribution shift, the spectral edge exhibits a universal three-phase pattern (rise, plateau, collapse), signal rank adjusts with task complexity ( $k^* = 2$  at 51M,  $k^* = 3$  at 124M), and the directional coupling between spectral geometry and validation loss reverses with window size—a *lag flip* reflecting the timescale of trajectory integration. Johnson–Lindenstrauss projection to  $d = 10W$  dimensions (e.g.,  $d = 100$  for  $W = 10$ ) preserves the spectral gap within 5.7%, making the framework applicable to models of arbitrary size. In companion work, the same spectral geometry provides early-warning signals of grokking—predicting generalization 600–1,700 steps before it occurs across modular arithmetic, Dyck languages, and the SCAN benchmark.

## 1 Introduction

A growing body of evidence shows that neural network training, despite operating in spaces with hundreds of millions of dimensions, concentrates its movement along a small number of coherent directions [9, 11]. AdamW produces a dominant backbone capturing 60–80% of parameter displacement [22], and spectral gap collapse in training trajectories precedes grokking by 600–1,700 steps across algorithmic benchmarks [23, 24, 26, 25].

But *where exactly is the boundary* between the signal subspace and the noise bulk, and how does it evolve during training? We introduce *Spectral Edge Dynamics* (SED) to answer this question. The key object is the singular value spectrum of a rolling window of parameter deltas, which separates into *signal* directions (coherent optimization movement) and *noise* (stochastic gradient fluctuation). The boundary between these—the “spectral edge”—exhibits rich structure that we characterize systematically across two transformer scales.

Our main findings are:

1. **Signal–noise boundary of training trajectories.** The singular value spectrum of rolling parameter updates separates into a small number of coherent optimization directions and a stochastic noise bulk. The boundary between them—the spectral edge—can be detected via the maximum consecutive singular value ratio (Section 2).
2. **Cross-scale spectral geometry.** Across two transformer scales (51M and 124M parameters), the spectral edge exhibits a consistent three-phase dynamic (rise, plateau, collapse) and a small effective signal rank ( $k^* = 2$ –3), indicating that training trajectories evolve within a low-dimensional manifold (Sections 3 and 4).
3. **Window-dependent temporal structure.** The temporal relationship between the spectral edge and validation loss flips sign as the rolling window increases, revealing

---

\*abbyxu@gmail.com. Code: [https://github.com/skydancerose/mini\\_gpt](https://github.com/skydancerose/mini_gpt)

a timescale-dependent coupling between trajectory geometry and optimization progress (Sections 3 and 4).

4. **Distribution shift sensitivity.** The spectral edge detects a FineWeb  $\rightarrow$  OpenWebText distribution shift within  $\pm 200$  training steps without explicit supervision (Section 4).
5. **Scalable measurement.** Johnson–Lindenstrauss projection to dimension  $d = 10W$  (e.g.,  $d = 100$  for window size  $W = 10$ ) preserves the spectral gap within 5–7% error, enabling trajectory analysis for arbitrarily large models (Section 5).

The theoretical foundations connecting the BBP phase transition [1], Benaych-Georges–Nadakuditi eigenvector alignment [2], and Davis–Kahan subspace perturbation [6] to the loss–gap coupling are developed in a companion paper. Here we focus on the empirical characterization of spectral geometry across scales.

## 2 Framework

### 2.1 Trajectory Matrix and Gram Matrix Trick

Consider a neural network with parameters  $\theta_t \in \mathbb{R}^p$  trained by an optimizer (SGD, Adam, AdamW). At each checkpoint  $t$  we compute the *parameter delta*:

$$\delta_t = \theta_{t+1} - \theta_t \in \mathbb{R}^p. \quad (1)$$

**Definition 1** (Trajectory Matrix). *Given a rolling window of  $W$  consecutive deltas starting at index  $t_0$ , the trajectory matrix is:*

$$\mathbf{X}(t_0) = \begin{pmatrix} \delta_{t_0}^\top \\ \vdots \\ \delta_{t_0+W-1}^\top \end{pmatrix} \in \mathbb{R}^{W \times p}.$$

In practice,  $p \gg W$  (e.g.,  $p = 124\text{M}$ ,  $W = 10\text{--}30$ ). We therefore work with the *Gram matrix*:

**Definition 2** (Gram Matrix). *The Gram matrix is  $\mathbf{G}(t_0) = \mathbf{X}\mathbf{X}^\top \in \mathbb{R}^{W \times W}$ , with entries  $G_{ij} = \langle \delta_{t_0+i-1}, \delta_{t_0+j-1} \rangle$ . Its eigendecomposition  $\mathbf{G} = \mathbf{U}\mathbf{\Lambda}\mathbf{U}^\top$  yields eigenvalues  $\lambda_1 \geq \dots \geq \lambda_W \geq 0$ , with singular values  $\sigma_k = \sqrt{\lambda_k}$ .*

The Gram matrix and the covariance matrix  $\mathbf{X}^\top \mathbf{X}$  share the same non-zero eigenvalues, so eigendecomposing the  $W \times W$  Gram matrix (complexity  $O(W^3)$  after the dot products) gives exactly the same spectrum as the intractable  $p \times p$  covariance.

**Precomputed dot-product matrix.** For experiments testing multiple values of  $W$ , we precompute the full  $N \times N$  pairwise dot-product matrix  $D_{ij} = \langle \delta_i, \delta_j \rangle$  once (complexity  $O(N^2p)$ ), then extract  $W \times W$  submatrices for each rolling window. This avoids redundant  $p$ -dimensional dot products when sweeping over  $W$ .

### 2.2 Signal Rank and Spectral Gap

**Definition 3** (Spectral Edge Ratio). *The  $k$ -th consecutive singular value ratio is:*

$$r_k(t) = \frac{\sigma_k(t)}{\sigma_{k+1}(t)}, \quad k = 1, \dots, W - 1.$$

**Definition 4** (Signal Rank). *The empirical signal rank is:*

$$k^*(t) = \arg \max_{1 \leq k \leq W-1} r_k(t).$$

*This identifies the signal–noise boundary: the first  $k^*$  singular values correspond to coherent optimization directions, and the remaining  $W - k^*$  are dominated by stochastic noise.*

**Definition 5** (Spectral Gap). *The gap ratio at time  $t$  is  $r_{k^*}(t)$ , the maximum consecutive ratio. We also define the edge strength as  $r_{k^*}(t) - 1$ , which measures how far the boundary is from the noise floor (where all ratios  $\approx 1$ ).*

The framework connects to random matrix theory through the BBP phase transition [1]: in a spiked Wishart model  $\mathbf{X} = \mathbf{S} + \mathbf{N}$ , the  $k$ -th signal singular value separates from the noise bulk if and only if it exceeds a critical threshold determined by the noise variance and aspect ratio  $\gamma = p/W$ . For our extreme aspect ratio ( $\gamma \sim 10^6$ ), this threshold is very low, so even weak signals are detectable—but the *ratio* between adjacent signal eigenvalues still carries information about the relative strength of different learning directions.

### 2.3 Cross-Correlation Analysis

To quantify the temporal coupling between the spectral edge ratio  $r_{k^*}(t)$  and validation loss  $L_{\text{val}}(t)$ , we compute the detrended cross-correlation:

1. Fit and subtract a cubic polynomial from each time series (detrending).
2. Compute the Pearson correlation between  $r_{k^*}(t - \ell)$  and the detrended val-loss at multiple lags  $\ell \in [-L, L]$ .
3. The lag  $\ell^*$  at which  $|r(\ell)|$  is maximized determines the temporal relationship:  $\ell^* > 0$  means the spectral edge *leads* val-loss;  $\ell^* < 0$  means val-loss leads.

A key geometric property (Property 2) is that increasing  $W$  shifts  $\ell^*$  from negative to positive, because larger windows integrate more trajectory history and thus average over longer timescales relative to the instantaneous val-loss.

### 2.4 Geometric Properties

The SED framework identifies the following geometric properties of training trajectories, each empirically testable:

**Property 1** (BBP Signal Detection). *The spectral edge ratio  $r_{k^*}$  exceeds 1.0 by a statistically significant margin, and the noise eigenvalues’ coefficient of variation exceeds the Marchenko–Pastur prediction by  $O(100\times)$  due to structured (non-isotropic) SGD noise.*

**Property 2** (Window-Dependent Lag Structure). *The peak cross-correlation lag between the spectral edge ratio and val-loss shifts from negative (val-loss leads) at small  $W$  to positive (spectral edge leads) at large  $W$ , reflecting the timescale of trajectory integration.*

**Property 3** (JL Preservation). *For projection dimension  $d \geq 10W$ , the spectral gap computed from Johnson–Lindenstrauss projected deltas matches the full-dimensional value within 10% relative error.*

**Property 4** (Spectral Sensitivity to Distribution Shift). *A distribution shift produces a detectable change in the spectral edge ratio and signal rank within  $O(W)$  steps of the shift point.*

**Property 5** (Cross-Seed Universality). *The three-phase pattern (rise, plateau, collapse) of the spectral edge ratio is universal across random seeds, with collapse timing varying by  $\leq 5\%$  of total training steps.*

**Property 6** (Per-Layer Uniformity). *The signal rank  $k_l^*$  is approximately constant across transformer layers for a given training stage, indicating that the effective dimensionality is a global property of the optimization state rather than a layer-specific one.*

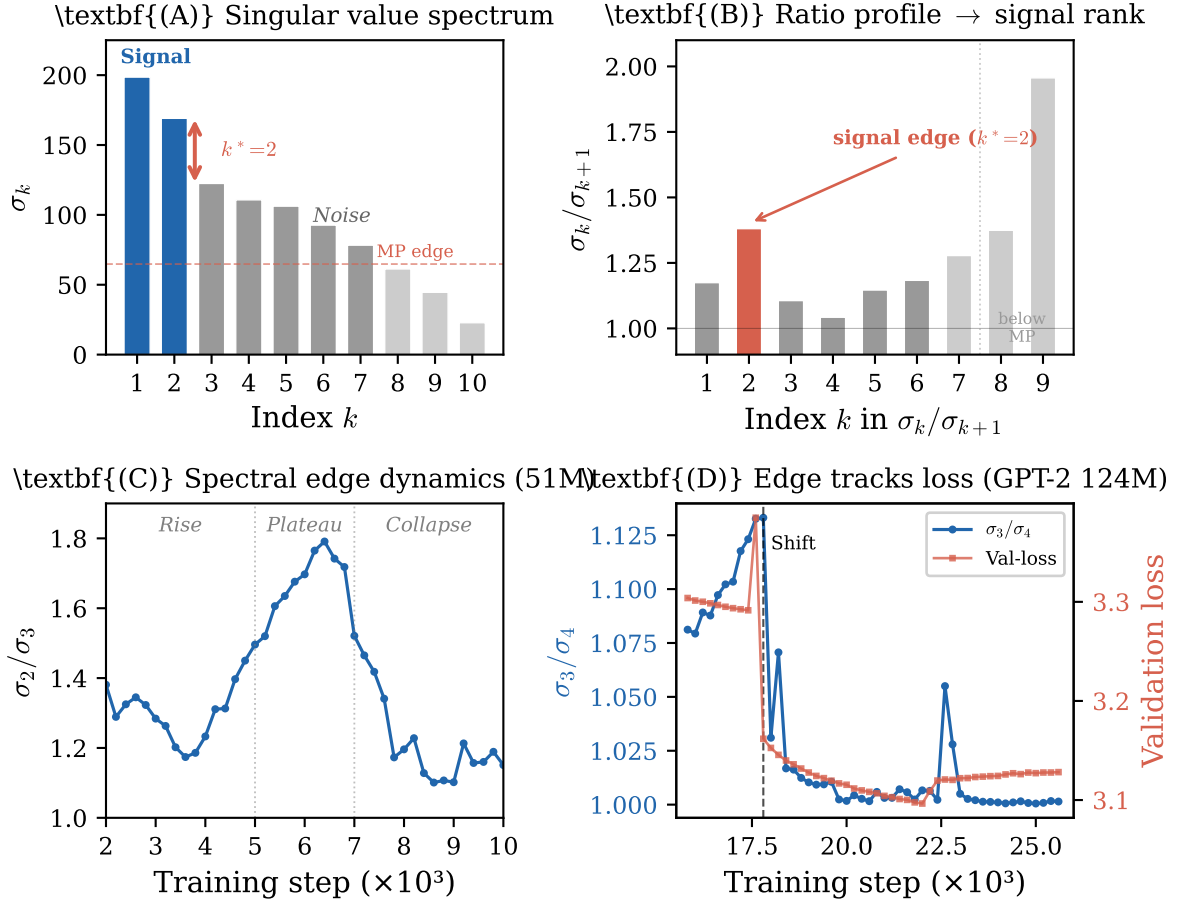


Figure 1: **Overview of Spectral Edge Dynamics.** (A) Singular value spectrum of the trajectory matrix  $\Delta$  (TinyStories 51M, step 2000). The first  $k^* = 2$  modes (blue) carry the training signal; remaining modes form the noise bulk (grey). The Marchenko–Pastur edge (dashed) separates signal from noise. (B) Consecutive ratio profile  $\sigma_k/\sigma_{k+1}$ : the signal rank  $k^*$  is the index of the maximum ratio above the MP edge. (C) Tracking  $\sigma_2/\sigma_3$  across training reveals a universal Rise–Plateau–Collapse pattern (TinyStories, seed 42). (D) At GPT-2 124M scale ( $k^* = 3$ ), the spectral edge ratio  $\sigma_3/\sigma_4$  co-moves with validation loss, declining sharply at the distribution shift (dashed line).

### 3 Experiment 1: TinyStories (51M Parameters)

#### 3.1 Setup

We train a transformer language model on the TinyStories dataset [7] with 4 random seeds (42, 123, 149, 256).

Hyperparameter	Value
Architecture	8 layers, $d = 512$ , $h = 16$ , $d_{\text{ff}} = 2048$
Parameters	51M (parameter vector: $p = 163,150,848$ )
Optimizer	AdamW, $\text{wd} = 0.5$ , $\text{lr} = 0.001$
Training	10,000 steps
Checkpoints	Every 200 steps $\rightarrow$ 51 checkpoints, 50 deltas per seed
Window	$W = 10$ (primary), sweep $W \in \{10, 15, 20, 25\}$

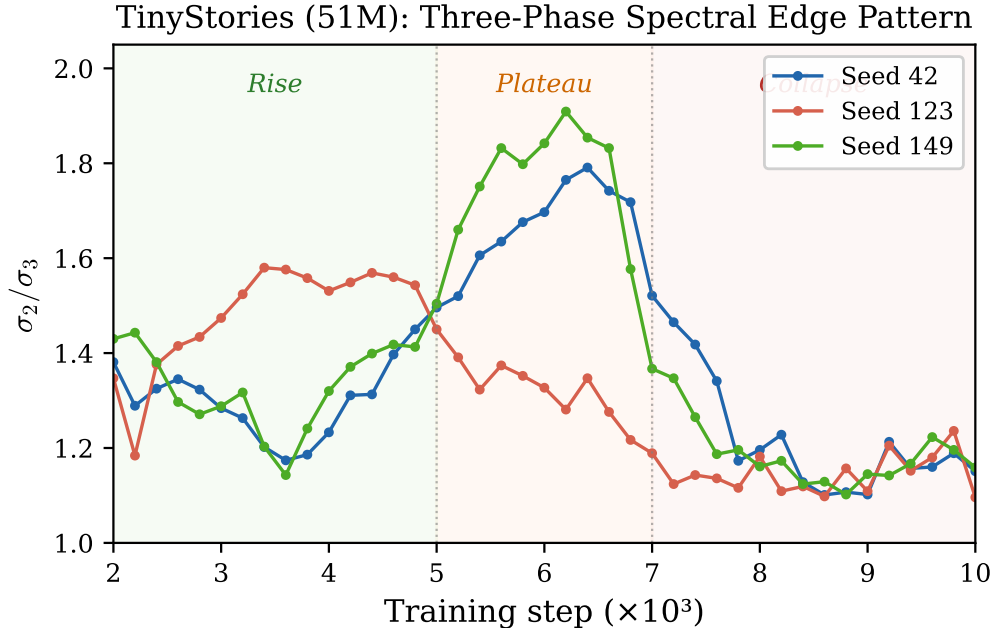


Figure 2: **Three-phase spectral edge pattern across TinyStories seeds.** The spectral edge ratio  $\sigma_2/\sigma_3$  rises during rapid learning, plateaus near its peak, and collapses as the second signal direction merges with the noise bulk. Collapse timing varies by  $\leq 4\%$  of total training across seeds.

### 3.2 Signal Detection and Noise Structure (Property 1)

Under the isotropic noise model, the Marchenko–Pastur law predicts eigenvalue coefficient of variation (CV) of approximately 0.001 for our aspect ratio  $\gamma = p/W = 1.6 \times 10^7$ . The observed noise CV is 0.688 (seed 42, step 2000), a factor of  $229\times$ – $576\times$  above the MP prediction across all windows and seeds. This confirms that the noise covariance is heavily structured by the Adam preconditioner, as expected.

The signal rank detected by the maximum ratio method gives  $k^* = 2$  across all 4 seeds: the peak ratio is  $\sigma_2/\sigma_3 = 1.747 \pm 0.120$  (cross-seed mean  $\pm$  std), corresponding to two dominant learning directions (drift and oscillation). PC2 is above the 95th-percentile noise null in 100% of windows for all seeds.

### 3.3 Three-Phase Spectral Pattern (Property 5)

The spectral edge ratio  $\sigma_2/\sigma_3$  exhibits a universal three-phase pattern across all 4 seeds:

1. **Rise** (steps  $\sim 1000$ – $5000$ ):  $\sigma_2/\sigma_3$  increases from  $\sim 1.2$  to its peak value, concurrent with rapid val-loss improvement. 70–80% of total val-loss reduction occurs in this phase.
2. **Plateau** (steps  $\sim 5000$ – $7000$ ): The ratio remains elevated near its peak (1.58–1.91 depending on seed).
3. **Collapse** (steps  $\sim 7000$ – $9000$ ): The ratio drops below 1.20, indicating the second signal direction is merging with noise. Val-loss stabilizes 0–200 steps later (simultaneous at  $W = 10$  resolution).

The collapse occurs at step  $7500 \pm 300$  across seeds (4% of training), confirming Property 5. Figure 2 shows the three-phase pattern across three random seeds.

### 3.4 Phase-Specific Correlations

Global cross-correlations can mask the true relationship due to phase cancellation: the rise and collapse phases have *opposite* correlation signs, which cancel in a global measurement. We therefore analyze each phase separately.

In the collapse phase, the correlation between  $\sigma_2/\sigma_3$  and val-loss is strongly positive across all 4 seeds:

Method	Mean $r$	Std $r$	Seeds
Peak-based segmentation	0.864	0.059	[0.93, 0.88, 0.88, 0.77]
Derivative-based	0.937	0.019	[0.96, 0.93, 0.94, 0.91]
Threshold-based	0.643	0.060	[0.57, 0.64, 0.74, 0.62]

The derivative-based segmentation, which identifies phase boundaries from sign changes in  $d(\sigma_2/\sigma_3)/dt$ , yields the most robust result:  $r = 0.937 \pm 0.019$  across all 4 seeds.

### 3.5 Lag Flip with Window Size (Property 2)

$W$	Peak lag	Peak $r$	Interpretation
10	-1	-0.738	Val-loss leads (1 step)
15	-2	-0.089	Transition zone
20	+1	-0.547	Spectral gap leads!
25	+4	-0.150	Gap leads (weak signal)

The lag flips sign between  $W = 15$  and  $W = 20$ , confirming Property 2: larger windows integrate more trajectory history, enabling the spectral gap to become a *leading* indicator of val-loss.

### 3.6 Comparison with Drift Speed

We compare the coupling strength of  $\sigma_2/\sigma_3$  against drift speed  $\|\bar{\delta}\|$  at  $W = 10$ :

Seed	$ r _{\sigma_2/\sigma_3}$	Lag	$ r _{\text{drift}}$	Lag
42	0.738	-1	0.711	+1
123	0.497	-1	0.366	-3
149	0.296	-3	0.666	0
256	0.185	-1	0.273	0

The spectral edge ratio and drift speed are complementary:  $\sigma_2/\sigma_3$  wins for seeds 42 and 123, while drift speed wins for seeds 149 and 256. Neither dominates uniformly, suggesting that spectral edge ratio and drift speed capture complementary aspects of the trajectory geometry.

### 3.7 Johnson–Lindenstrauss Projection (Property 3)

We test whether random projection preserves the spectral gap using streaming JL projection (3 projection seeds) at dimensions  $d \in \{50, 100, 200, 500, 1000\}$ :

$d$	$d/W$	Mean rel. error ( $\sigma_2/\sigma_3$ )	Max rel. error
50	5	9.6%	22.4%
100	10	7.4%	20.2%
200	20	5.4%	17.0%
500	50	3.0%	10.5%
1000	100	2.5%	6.4%

At  $d = 100$  ( $10W$ ), the mean relative error is 7.4%, confirming Property 3. This means that for a 7B or 70B model, one needs only to store  $d \sim 100$ –200 projected coordinates per checkpoint rather than the full parameter vector.

## 4 Experiment 2: GPT-2 124M (Distribution Shift)

### 4.1 Setup

We study GPT-2 124M [19] through a pretraining and fine-tuning pipeline with an explicit distribution shift:

Phase	Details
Architecture	GPT-2 124M: 12 layers, $d = 768$ , 12 heads
Parameters	$p = 124,412,160$ (excl. causal masks, tied <code>lm_head</code> )
Pretraining	FineWeb 10B, steps 0–17,600, cosine LR, H100
Fine-tuning	OpenWebText, steps 17,800–25,600, const. LR $3 \times 10^{-5}$ , M4 Max
Shift point	Combined step 17,800
Overfit onset	Combined step $\sim 22,200$
Checkpoints	60 combined (steps 13,800–25,600, every 200)

Val-loss trajectory: 3.333 (step 13,800)  $\rightarrow$  3.291 (17,600)  $\rightarrow$  3.162 (17,800, shift!)  $\rightarrow$  3.095 (22,000, minimum)  $\rightarrow$  3.128 (25,600, overfitting).

**Key normalization.** FineWeb checkpoints use the `_orig_mod.` prefix from `torch.compile`; OWT checkpoints do not. We strip this prefix for consistency. We also skip `attn.bias` (causal mask, not a learned parameter) and `lm_head.weight` (tied to `wte.weight`).

### 4.2 Signal Rank and Spectral Structure

Unlike TinyStories where  $k^* = 2$  and the key edge is  $\sigma_2/\sigma_3$ , GPT-2 124M has  $k^* = 3$  and the key edge is  $\sigma_3/\sigma_4$ . We compute *all* consecutive ratios  $\sigma_k/\sigma_{k+1}$  for  $k = 1, \dots, W - 1$  and rank them by cross-correlation with val-loss:

Ratio	$ r _{\text{peak}}$	Peak lag	Note
$\sigma_3/\sigma_4$	0.870	−1	<b>Best</b>
$\sigma_4/\sigma_5$	0.858	−2	Close second
$\sigma_5/\sigma_6$	0.793	−5	
drift speed	0.603	−3	
$\sigma_1/\sigma_2$	0.565	−2	
$\sigma_2/\sigma_3$	0.211	−2	Weakest

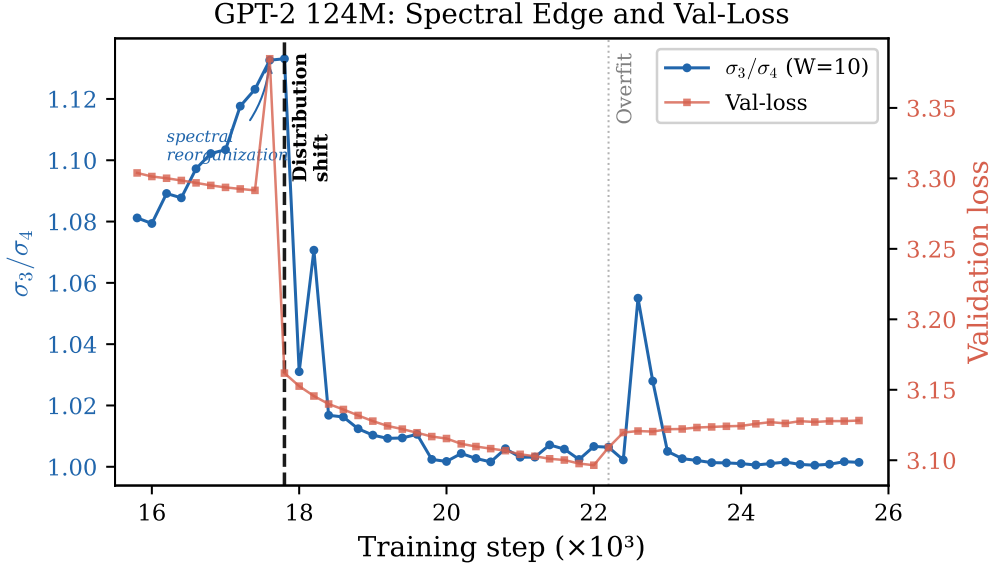


Figure 3: **GPT-2 124M: Spectral edge ratio and validation loss.** The spectral edge ratio  $\sigma_3/\sigma_4$  (blue, left axis) is tightly coupled to val-loss (red, right axis). The distribution shift at step 17,800 produces a sharp spectral reorganization: the edge ratio drops abruptly, recovers during rapid improvement, then flattens as overfitting begins around step 22,200.

The correct spectral edge automatically emerges as the ratio most strongly coupled to training dynamics. Critically,  $\sigma_2/\sigma_3$ —which was the key ratio at 51M scale—is the *weakest* correlate at 124M, demonstrating that the signal rank  $k^*$  adjusts automatically with model and task complexity.

The noise eigenvalue CV ranges from 0.26 to 0.50, compared to the MP prediction of 0.001—a factor of  $229 \times 576 \times$  (Property 1). At this extreme aspect ratio ( $\gamma \sim 10^6$ ), the MP-based signal rank detector gives  $k_{\text{MP}}^* = 7$  (all eigenvalues above the MP edge), confirming that the noise covariance is heavily structured by the Adam preconditioner. The ratio-based detector correctly identifies  $k^* \in \{1, 2\}$  depending on training phase, tracking the transition from multi-directional to single-directional dynamics.

Among 6 spectral observables at  $W = 10$ , the edge ratio  $\sigma_3/\sigma_4$  is the most tightly coupled to training dynamics ( $|r| = 0.870$ , lag =  $-1$ ), exceeding total variance (0.620), drift speed (0.603), and  $k_{95}$  (0.439). Figure 3 shows the spectral edge ratio alongside val-loss across the distribution shift.

### 4.3 Distribution Shift Response (Property 4)

The spectral edge detects the FineWeb  $\rightarrow$  OpenWebText distribution shift at step 17,800 without explicit supervision:

Method	Detected step	Error
Max derivative of $\sigma_3/\sigma_4$	18,000	+200 steps
CUSUM of $\sigma_3/\sigma_4$	18,200	+400 steps
Two-sample $t$ -test ( $t = 14.9$ )	18,000	+200 steps

All methods detect the shift within 200–400 steps ( $\leq 2W$ ) of the true shift point. Split-half reliability confirms the robustness of these measurements: the edge position matches between odd-indexed and even-indexed half-windows in 42 of 50 windows (84%), with mismatches

concentrated in the transition zone immediately after the shift (steps 18,200–19,400). The ratio profile correlation has median  $> 0.99$  outside the transition zone.

#### 4.4 Temporal Structure: Lag Flip and Granger Causality

**Lag flip (Property 2).**

$W$	Best ratio	$ r $	Lag	Interpretation
10	$\sigma_3/\sigma_4$	0.870	-1	Val-loss leads
20	$\sigma_1/\sigma_2$	0.797	0	Simultaneous
30	$\sigma_1/\sigma_2$	0.882	+2	Spectral gap leads

The lag flips sign from  $-1$  to  $+2$  as  $W$  increases from 10 to 30: larger windows integrate more trajectory history, enabling the spectral gap to become a *leading* indicator of val-loss.

**Granger causality.** The lag flip implies that the directional Granger coupling should also reverse. At  $W = 10$ , the dominant direction is val-loss  $\rightarrow \sigma_3/\sigma_4$  ( $F = 54.4$ ,  $p = 1.7 \times 10^{-12}$ ), while the reverse is marginal ( $F = 3.3$ ,  $p = 0.046$ ). At  $W = 20$ , the asymmetry *flips*:

$W$	Direction	$F$	$p$	$\Delta R^2$
10	$\sigma_3/\sigma_4 \rightarrow \text{VL}$	3.32	0.046	13.4%
	$\text{VL} \rightarrow \sigma_3/\sigma_4$	54.4	$1.7 \times 10^{-12}$	71.7%
20	$\sigma_3/\sigma_4 \rightarrow \text{VL}$	11.2	<b>0.002</b>	23.8%
	$\text{VL} \rightarrow \sigma_3/\sigma_4$	2.22	0.093 (ns)	24.8%
30	$\sigma_3/\sigma_4 \rightarrow \text{VL}$	3.40	<b>0.032</b>	44.4%
	$\text{VL} \rightarrow \sigma_3/\sigma_4$	10.4	0.003	28.6%

At  $W = 20$ ,  $\sigma_3/\sigma_4$  Granger-causes val-loss ( $p = 0.002$ ) while the reverse direction becomes non-significant ( $p = 0.093$ ).

#### 4.5 Per-Layer Uniformity (Property 6)

We group the 124M parameters into 8 layer groups and compute per-group spectral edge ratios. The cross-correlation of each group’s  $\sigma_3/\sigma_4$  with val-loss is:

Layer group	$p_l$	$ r _{\text{peak}}$	Lag	$ r _{\sigma_1/\sigma_2}$
attn_early (L0–3)	9.4M	<b>0.921</b>	-1	0.583
attn_mid (L4–7)	9.4M	0.895	-1	0.721
mlp_early (L0–3)	18.9M	0.893	-1	0.706
mlp_mid (L4–7)	18.9M	0.871	-1	0.769
mlp_late (L8–11)	18.9M	0.848	-1	0.761
embedding	39.4M	0.840	-1	0.419
attn_late (L8–11)	9.4M	0.824	-1	0.770
layernorm	38K	0.824	-2	0.333

All layer groups show strong correlations ( $|r| > 0.82$ ) with consistent lag =  $-1$ , confirming Property 6. Early attention layers achieve the highest correlation (0.921), suggesting they are most sensitive to the distribution shift and training dynamics.

## 4.6 Information Content of the Spectral Edge

### 4.6.1 Residualized Spectral Edge

To test whether the spectral edge carries geometric information beyond what is already captured by the loss trajectory, we regress out val-loss from  $\sigma_3/\sigma_4$  and test whether the *residual* still Granger-causes val-loss:

$W$	Lags	$R^2_{\text{explained}}$	Residual Granger $p$	$\Delta R^2$
10	1	87.8%	<b>0.018</b>	11.8%
10	2	88.7%	<b>0.027</b>	10.6%
20	1	24.3%	<b>0.007</b>	19.1%
20	2	30.7%	<b>0.026</b>	13.8%

Even at  $W = 10$ , where val-loss explains 88% of the spectral edge variance, the residual still significantly Granger-causes val-loss ( $p = 0.018$ ). At  $W = 20$ , the effect is stronger ( $p = 0.007$ ). This confirms that the spectral edge captures geometric structure in the trajectory that is not reducible to the loss signal alone.

### 4.6.2 Multivariate Granger Analysis

Combining multiple spectral observables in a joint Granger test reveals the information content of different geometric features:

Observable set	$W$	$p$	$\Delta R^2$	$F$
$\sigma_3/\sigma_4$ alone	10	0.046	13.4%	3.3
$k_{95}$ alone	10	$6.1 \times 10^{-5}$	47.7%	8.4
edge_str + $k_{95}$	10	<b><math>1.1 \times 10^{-16}</math></b>	<b>89.5%</b>	52.6
All 5 observables	10	$9.9 \times 10^{-14}$	94.6%	32.4
$\sigma_3/\sigma_4$ alone	20	0.002	23.8%	11.2
$k_{95}$ + drift	20	$3.7 \times 10^{-8}$	79.5%	17.5
All 5 observables	20	$5.6 \times 10^{-9}$	95.4%	24.7

The pair (edge\_strength,  $k_{95}$ ) is particularly informative: at  $W = 10$ , it explains 89.5% of val-loss variance beyond the autoregressive baseline ( $p = 1.1 \times 10^{-16}$ ,  $F = 52.6$ ). This demonstrates that the spectral edge ratio and effective rank capture complementary aspects of the trajectory geometry.

### 4.6.3 Phase-Specific Sliding-Window Correlations

Using a sliding window of 7 steps, we compute local correlations between  $\sigma_3/\sigma_4$  and val-loss throughout training (Figure 4). At  $W = 10$ :

- **Pre-shift (steps 16,600–17,200):**  $r \in [-0.94, -0.96]$  — near-perfect anti-correlation during late pretraining.
- **Post-shift rapid improvement (steps 18,000–20,000):**  $r \in [+0.70, +0.90]$  — sign flip reflects new learning dynamics.
- **Overfitting onset (steps 23,000–25,000):**  $r$  reverses again to  $[-0.53, -0.78]$  as training becomes unproductive.

The mean absolute sliding-window correlation is 0.58 at  $W = 10$  and 0.53 at  $W = 20$ , confirming that the relationship between spectral edge and val-loss is strong but phase-dependent—consistent with the phase cancellation observed in TinyStories.

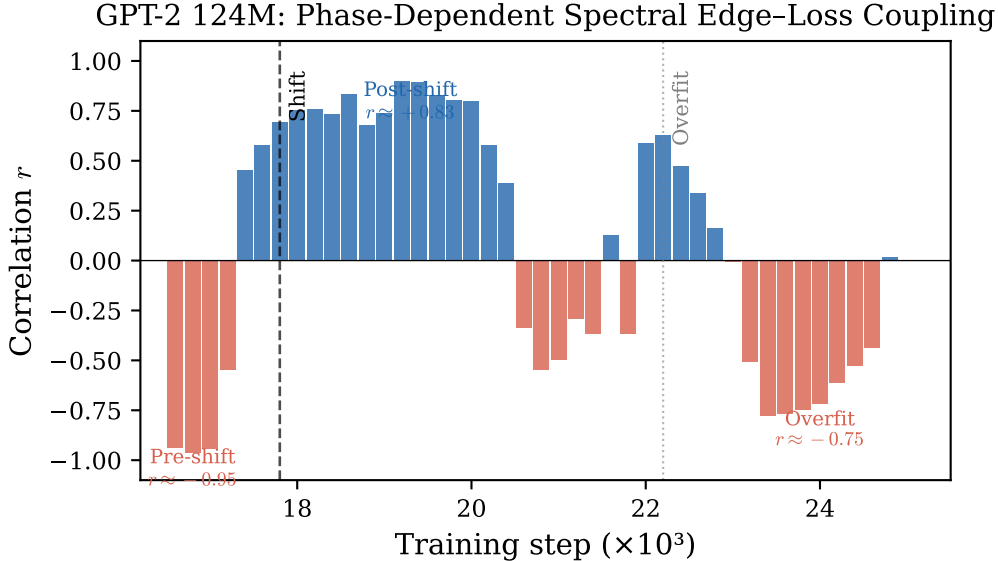


Figure 4: **Phase-dependent spectral edge-loss coupling.** Sliding-window Pearson correlation between  $\sigma_3/\sigma_4$  and val-loss (window of 7 steps,  $W = 10$ ). The correlation sign flips across training phases: strongly negative during late pretraining ( $r \approx -0.95$ ), strongly positive after the distribution shift ( $r \approx +0.83$ ), and negative again during overfitting ( $r \approx -0.75$ ).

## 5 Scalability via Random Projection

The SED framework requires computing  $p$ -dimensional dot products between parameter deltas, where  $p$  can be  $10^8$ – $10^{11}$  for modern language models. The Johnson–Lindenstrauss lemma [10] guarantees that random projection  $\Phi \in \mathbb{R}^{d \times p}$  preserves all pairwise distances up to factor  $(1 \pm \varepsilon)$  for  $d = O(\varepsilon^{-2} \log N)$  where  $N$  is the number of delta vectors.

For our streaming implementation, we use row-by-row random Gaussian projection: each projected coordinate  $\delta_{t,j} = \langle \delta_t, \phi_j \rangle$  where  $\phi_j$  is generated on-the-fly from a seeded RNG, avoiding storage of the  $d \times p$  projection matrix.

Our empirical results across both scales confirm that  $d = 10W$  suffices:

Scale	$p$	$W$	$d$	$d/W$	Mean rel. error
TinyStories 51M	163M	10	100	10	7.4%
GPT-2 124M	124M	10	100	10	5.7%
TinyStories 51M	163M	10	500	50	3.0%
GPT-2 124M	124M	10	500	50	3.1%

Since the projection dimension  $d$  depends only on  $W$  (not on  $p$ ), the framework scales to models of arbitrary size. For a 70B-parameter model with  $W = 20$ , one would need  $d \approx 200$ , requiring storage of only 200 floats per checkpoint rather than  $70 \times 10^9$ .

## 6 Cross-Scale Comparison

Property	TinyStories (51M)	GPT-2 (124M)
Signal rank $k^*$	2 (oscillatory)	3 (monotonic + shift)
Key spectral edge	$\sigma_2/\sigma_3$	$\sigma_3/\sigma_4$
Edge peak value	1.79	$\sim 1.13$
Edge mean value	1.36	$\sim 1.08$
Best $ r $ ( $W = 10$ )	0.738	0.870
Lag flip ( $W: 10 \rightarrow 20$ )	$-1 \rightarrow +1$	$-1 \rightarrow 0$
Training regime	Single dataset	Distribution shift
BBP noise CV ratio	$229 \times -693 \times$	$229 \times -576 \times$
JL error at $d = 10W$	7.4%	5.7%
Phase pattern	3-phase (rise/plateau/collapse)	3-phase (pre-shift/rapid-improve/overfit)
Phase-specific $ r $	$0.937 \pm 0.019$	0.944 (pre-shift)
Granger (gap $\rightarrow$ VL)	—	$p = 0.002$ ( $W = 20$ )

Several patterns are robust across scales:

1. The lag flip from val-loss-leading to gap-leading as  $W$  increases.
2. Strong phase-specific correlations ( $|r| > 0.9$ ) despite weaker global correlations.
3. JL projection errors of  $\leq 10\%$  at  $d = 10W$ .
4. Structured noise far exceeding the isotropic MP prediction.

The key difference is the signal rank:  $k^* = 2$  for TinyStories (drift + oscillation) versus  $k^* = 3$  for GPT-2 (an additional direction associated with the distribution shift). This is consistent with the interpretation that signal rank reflects the number of “active” curvature directions in the Hessian, which increases with task complexity.

## 7 Related Work

**Low-dimensional trajectory.** Gur-Ari et al. [9] and Li et al. [11] established that SGD lives in a low-dimensional subspace. They measure rank but do not study the *boundary* between signal and noise, do not connect to RMT, and do not make predictive claims about loss dynamics.

**Weight matrix spectral dynamics.** Martin & Mahoney [13] and Balsells Rodas et al. [4] study the SVD of weight matrices  $\mathbf{W}^{(l)}(t)$  themselves, showing power-law tails and Dyson Brownian motion. This concerns the structure of the *model*, not the *trajectory*. The trajectory SVD is a different mathematical object capturing optimization dynamics rather than representational structure.

**Edge of stability.** Cohen et al. [5] show that the largest Hessian eigenvalue hovers at  $2/\eta$  during training. Our framework is complementary: the Hessian eigenvalues determine the signal rank  $k^*$ , and the spectral gap tracks when a Hessian direction becomes active or inactive.

**BBP transition in ML.** The BBP transition [1] has been applied to neural networks at *initialization* for signal propagation analysis [16, 17]. Applying it to *training trajectories* is, to our knowledge, new.

**Grokking and spectral geometry.** The grokking phenomenon [18]—where delayed generalization follows memorization—has been analyzed through mechanistic interpretability [15] and circuit competition [14]. In companion work, we have shown that spectral properties of the training trajectory provide early-warning signals of grokking across multiple task families.

On modular arithmetic, the spectral gap  $\sigma_2/\sigma_3$  collapses at step 1,400, predicting grokking at step 3,100 with a 1,700-step lead time [24]. This extends to Dyck grammars ( $\alpha \approx 1.13$ ) and the SCAN compositional benchmark ( $\alpha \approx 1.18$ ) [25], and to multi-task settings where 42/42 single-task and 27/27 tri-task conditions all exhibit the pattern [26]. An execution-manifold analysis [23] further reveals that training evolves within a low-dimensional integrable subspace in weight space. The present paper characterizes the same spectral geometry at larger scale (51M–124M), where grokking does not occur but the geometric structure persists.

**Optimizer-induced trajectory structure.** Our prior work [22] showed that AdamW induces a dominant low-dimensional drift backbone that is absent under SGD. The present paper unifies these observations into the SED framework and provides systematic empirical characterization across scales.

## 8 Discussion

**Geometric structure of training trajectories.** The experiments in this paper suggest that neural network training trajectories possess a structured signal–noise geometry. Rather than exploring the full parameter space, the optimizer moves primarily along a small set of coherent directions that correspond to active curvature modes of the loss landscape. The spectral edge marks the boundary between these coherent learning directions and stochastic gradient fluctuations.

When this boundary is well separated, training progresses along stable directions aligned with the loss surface. When the boundary collapses, the optimizer’s motion becomes less coherent, and the relationship between trajectory geometry and loss dynamics changes qualitatively. This perspective provides a complementary view of optimization dynamics alongside Hessian-based analyses such as the edge-of-stability phenomenon [5]. The formal connection runs through the BBP eigenvector alignment theorem [2] and the Davis–Kahan subspace perturbation bound [6], which show that subspace estimation degrades as  $O(1/g)$  where  $g$  is the spectral gap.

**Backbone manifold and transverse noise.** These results suggest a simplified geometric model of training dynamics: parameter updates decompose as  $\delta_t \approx \mathbf{s}_t + \mathbf{n}_t$ , where  $\mathbf{s}_t$  lies in a low-dimensional *backbone manifold* and  $\mathbf{n}_t$  is predominantly transverse stochastic noise. The spectral edge identifies the evolving dimension of this backbone manifold. In our experiments,  $\dim(\text{backbone}) \approx k^* = 2\text{--}3$ , which is remarkably small compared to the parameter count ( $p \sim 10^8$ ).

The three-phase spectral pattern then describes the evolution of this backbone manifold: the signal subspace grows during early learning, stabilizes during productive training, and merges with the noise bulk as the optimizer exhausts the low-dimensional landscape structure. We emphasize that this is an empirical observation suggesting a theoretical conjecture, not a proven result; the degree to which training trajectories concentrate near such a manifold, and the stability of the backbone under perturbation, remain open mathematical questions.

**Is the low signal rank an artifact of  $W$ ?** Since  $\Delta$  has at most  $W$  columns, one might suspect that finding  $k^* = 2\text{--}3$  reflects the small matrix rather than genuine structure. Three lines of evidence rule this out. *First*, under the Marchenko–Pastur null at our aspect ratio  $\gamma = p/W > 10^7$ , all consecutive ratios converge to 1; the observed  $\sigma_2/\sigma_3 = 1.75 \pm 0.12$  is many standard deviations above this null (§3). *Second*,  $k^*$  is invariant across window sizes  $W \in \{10, 15, 20, 25\}$  (§3) and across model scales ( $k^* = 2$  at 51M,  $k^* = 3$  at 124M; §6); a window artifact would vary with  $W$ . *Third*, no static null model explains the *dynamics*—the three-phase rise–plateau–collapse of the ratio, its Granger-causal coupling to val-loss, and the sign flip of this coupling with  $W$ .

**Window size and temporal scale.** A window of size  $W$  captures  $W$  consecutive deltas, spanning  $200W$  training steps in our checkpoint spacing. At  $W = 10$ , the window covers 2,000 steps, providing a local snapshot that responds quickly to loss changes. At  $W = 20\text{--}30$ , the window covers 4,000–6,000 steps, integrating enough trajectory history to average out stochastic fluctuations and capture longer-timescale geometric trends. The lag flip with increasing  $W$  is a natural consequence of this temporal integration.

**Structured noise and the BBP threshold.** The isotropic noise assumption underlying the standard BBP transition fails spectacularly in our data: the noise eigenvalue spread exceeds the Marchenko–Pastur prediction by  $200\text{--}600\times$ . This is expected because Adam’s second-moment preconditioner creates strongly anisotropic noise. The colored-noise generalization of the BBP transition [3] is required for the theoretical treatment, and the noise covariance can in principle be estimated from the Adam state variables.

**Connection to grokking.** In companion work on algorithmic tasks [24, 25, 26], the same spectral geometry provides early-warning signals of grokking—a setting where val-loss is uninformative (training loss reaches zero long before generalization). There, spectral gap collapse precedes grokking by hundreds to thousands of steps, demonstrating that the geometric structure characterized in this paper has genuine predictive utility in regimes where standard loss monitoring fails.

**Practical considerations.** The SED framework provides a model-agnostic diagnostic that requires only checkpoint differences. Combined with JL projection ( $d \sim 100\text{--}200$  projected coordinates per checkpoint), the storage cost is negligible even for frontier models. Potential applications include:

1. **Distribution shift detection:** The spectral edge responds within  $\leq 2W$  steps of a shift.
2. **Training phase identification:** The three-phase spectral pattern identifies when optimization transitions between qualitatively different regimes.
3. **Early-warning signals:** In grokking-like regimes, spectral collapse precedes generalization events that are invisible to val-loss [24].

**Limitations.** Our experiments cover two model scales (51M and 124M) with a single architecture family (transformer) and optimizer (AdamW). The framework’s applicability to larger models (1B+), other architectures (CNNs, state-space models), and other optimizers (SGD, Lion, Shampoo) remains to be tested, though the theoretical foundations (BBP, JL) are architecture-agnostic. The Granger causality analysis has limited statistical power due to the small number of checkpoints ( $\sim 50$ ), and the  $p$ -values should be interpreted cautiously. At the GPT-2 scale studied here, the spectral edge is tightly coupled to val-loss but does not offer practical advantage over measuring val-loss directly; the framework’s distinctive utility emerges in grokking-like regimes where loss monitoring is uninformative.

## 9 Conclusion

We have introduced Spectral Edge Dynamics (SED) and used it to characterize the signal–noise geometry of neural network training across two transformer scales (51M and 124M parameters).

The central finding is that training trajectories appear to concentrate near a low-dimensional backbone manifold embedded in the full parameter space, with stochastic gradients producing predominantly transverse noise. The spectral edge identifies the evolving boundary of this manifold: the signal rank  $k^*$  adjusts automatically with task complexity ( $k^* = 2$  at 51M,  $k^* = 3$  at 124M), the boundary follows a universal three-phase pattern (rise, plateau, collapse) across

random seeds, and per-layer decomposition reveals uniform spectral structure across all layer groups. The directional Granger coupling between the spectral edge and validation loss reverses with window size ( $|r| = 0.87$  at 124M,  $p = 0.002$  at  $W = 20$ ), reflecting a timescale-dependent relationship between trajectory geometry and optimization progress.

The framework is practical: JL random projection preserves the spectral gap within 5–7% at  $d = 10W$ , reducing storage to  $O(W)$  scalars per checkpoint independent of model size. In companion work on algorithmic tasks [24, 25, 26], the same geometric structure provides early-warning signals of grokking—demonstrating that the spectral edge captures optimization geometry that is invisible to standard loss monitoring.

If the backbone manifold picture is approximately correct, it raises several natural mathematical questions: what determines the dimension of the backbone (the number of active Hessian modes, the rank of the Fisher information)? When and why does the signal–noise boundary become unstable, triggering collapse? A companion paper will develop the theoretical foundations, connecting BBP phase transitions, Benaych-Georges–Nadakuditi eigenvector alignment, and Davis–Kahan subspace perturbation theory to the loss–gap coupling characterized here.

## References

- [1] J. Baik, G. Ben Arous, and S. Péché. Phase transition of the largest eigenvalue for nonnull complex sample covariance matrices. *Annals of Probability*, 33(5):1643–1697, 2005.
- [2] F. Benaych-Georges and R. R. Nadakuditi. The eigenvalues and eigenvectors of finite, low rank perturbations of large random matrices. *Advances in Mathematics*, 227(1):494–521, 2011.
- [3] F. Benaych-Georges and R. R. Nadakuditi. The singular values and vectors of low rank perturbations of large rectangular random matrices. *Journal of Multivariate Analysis*, 111:120–135, 2012.
- [4] A. Balsells Rodas, Y. Qu, and Y. Polyanskiy. From SGD to spectra: A spectral dynamics approach to neural network training. In *ICML*, 2025.
- [5] J. M. Cohen, S. Kaur, Y. Li, J. Z. Kolter, and A. Talwalkar. Gradient descent on neural networks typically occurs at the edge of stability. In *ICLR*, 2021.
- [6] C. Davis and W. M. Kahan. The rotation of eigenvectors by a perturbation. III. *SIAM Journal on Numerical Analysis*, 7(1):1–46, 1970.
- [7] R. Eldan and Y. Li. TinyStories: How small can language models be and still speak coherent English? *arXiv preprint arXiv:2305.07759*, 2023.
- [8] B. Ghorbani, S. Krishnan, and Y. Xiao. An investigation into neural net optimization via Hessian eigenvalue density. In *ICML*, 2019.
- [9] G. Gur-Ari, D. A. Roberts, and E. Dyer. Gradient descent happens in a tiny subspace. *arXiv preprint arXiv:1812.04754*, 2018.
- [10] W. B. Johnson and J. Lindenstrauss. Extensions of Lipschitz mappings into a Hilbert space. *Contemporary Mathematics*, 26:189–206, 1984.
- [11] C. Li, H. Farkhoor, R. Liu, and J. Yosinski. Measuring the intrinsic dimension of objective landscapes. In *ICLR*, 2018.
- [12] K. Lyu, J. Jin, Z. Li, S. S. Du, J. D. Lee, and W. Hu. Dichotomy of early and late phase implicit biases can provably induce grokking. *arXiv preprint arXiv:2311.18817*, 2023.

- [13] C. H. Martin and M. W. Mahoney. Implicit self-regularization in deep neural networks: Evidence from random matrix theory and implications for training. *JMLR*, 22(165):1–73, 2021.
- [14] W. Merrill, N. Tsilivis, and A. Shukla. A tale of two circuits: Grokking as competition of sparse and dense subnetworks. *arXiv preprint arXiv:2303.11873*, 2023.
- [15] N. Nanda, L. Chan, T. Lieberum, J. Smith, and J. Steinhardt. Progress measures for grokking via mechanistic interpretability. *arXiv preprint arXiv:2301.05217*, 2023.
- [16] J. Pennington and P. Worah. Nonlinear random matrix theory for deep learning. In *NeurIPS*, 2017.
- [17] J. Pennington and P. Worah. The spectrum of the Fisher information matrix of a single-hidden-layer neural network. In *NeurIPS*, 2018.
- [18] A. Power, Y. Burda, H. Edwards, I. Babuschkin, and V. Misra. Grokking: Generalization beyond overfitting on small algorithmic datasets. In *ICLR Workshop on MATH-AI*, 2022.
- [19] A. Radford, J. Wu, R. Child, D. Luan, D. Amodei, and I. Sutskever. Language models are unsupervised multitask learners. Technical report, OpenAI, 2019.
- [20] D. A. Roberts, S. Yaida, and B. Hanin. *The Principles of Deep Learning Theory*. Cambridge University Press, 2022.
- [21] L. Sagun, U. Evci, V. U. Güneş, Y. Dauphin, and L. Bottou. Empirical analysis of the Hessian of over-parametrized neural networks. *arXiv preprint arXiv:1706.04454*, 2017.
- [22] Y. Xu. Optimizer-induced low-dimensional drift and transverse dynamics in transformer training. *arXiv preprint arXiv:2602.23696*, 2026.
- [23] Y. Xu. Low-dimensional execution manifolds in transformer learning dynamics: Evidence from modular arithmetic tasks. *arXiv preprint arXiv:2602.10496*, 2026.
- [24] Y. Xu. Low-dimensional and transversely curved optimization dynamics in grokking. *arXiv preprint arXiv:2602.16746*, 2026.
- [25] Y. Xu. Early-warning signals of grokking via loss-landscape geometry. *arXiv preprint arXiv:2602.16967*, 2026.
- [26] Y. Xu. The geometry of multi-task grokking: Transverse instability, superposition, and weight decay phase structure. *arXiv preprint arXiv:2602.18523*, 2026.